Chemical Engineering Journal 303 (2016) 331–337

Contents lists available at ScienceDirect

Chemical Engineering Journal

journal homepage: www.elsevier.com/locate/cej

Effect of particle size on copper removal by layered double hydroxides

Ricardo Rojas

INFIQC-CONICET, Departamento de Fisicoquímica, Facultad de Ciencias Químicas, Universidad Nacional de Córdoba. Ciudad Universitaria, 5000 Córdoba, Argentina

HIGHLIGHTS

- Mg^{2+} leaching in neutral media and congruent dissolution rate in acid boosted in nanoLDHs.
- At low Cu^{2+} concentrations, the pH buffering capacity of LDHs produce $Cu(OH)_2$ precipitation.
- In these conditions, nanoLDHs presented higher affinity for Cu^{2+} ions than microLDHs.
- At large Cu^{2+} concentrations, the sorption mechanism is isomorphic substitution of Mg^{2+} ions.
- NanoLDHs, due to their higher exposed surface, exhibited larger sorption capacities than microLDHs.

GRAPHICAL ABSTRACT

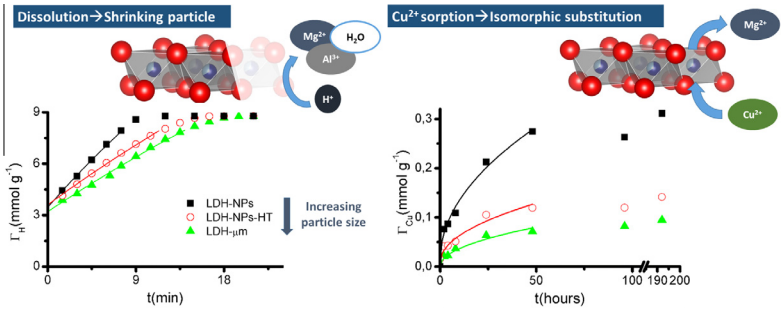

ARTICLE INFO

Article history:
Received 13 April 2016
Received in revised form 1 June 2016
Accepted 2 June 2016
Available online 3 June 2016

Keywords:
Heavy metal removal
Diadochy
Surface reactions
Kinetics
Isotherms

ABSTRACT

Layered double hydroxides are increasingly studied as heavy metal scavengers but the effect of particle size in their removal behavior has not been explored yet. Here, these aspects were studied in three solids with similar structure and composition but different in size and morphology. Nano-sized LDHs were synthesized by a coprecipitation method with separate nucleation and aging steps and compared to a micro-sized LDH. Proton and Cu^{2+} uptake were studied using both kinetics and isotherms, which were fitted using different models. Decreasing particle size caused an increasing Mg^{2+} leaching in neutral and basic media and an increased dissolution speed in acid media, both of them due to the larger exposed surface of smaller particles. Depending on the Cu^{2+} concentration and LDH buffering capacity, Cu^{2+} removal was produced by $Cu(OH)_2$ precipitation at the particle surface or by isomorphic substitution of Mg^{2+} ions at the octahedral sites of LDH layers (diadochy). The uptake rate of the latter was controlled by the intra-particle diffusion of Mg^{2+} ions and, consequently, it was quite independent of the particle size. On the other hand, the uptake capacity decreased with increasing particle size due to the site availability diminution with increasing diffusion path, which led to a decreasing volume of the layer available for Cu^{2+} uptake for increasing particle size values.

1. Introduction

Heavy metal ions, such as Cu^{2+}, Ni^{2+}, Pb^{2+} or Cd^{2+} represent a serious hazard due to their mobility, persistency and increasingly mobilization due to mining, plating and tanning activities [1]. These pollutants are remediated mainly by precipitation, ion exchange and adsorption processes [2,3] and materials such as activated carbon, zeolites, ion exchange resins, clays or layered double hydroxides (LDHs) are investigated as sorbents [4]. Also, the use of micro and nanomaterials generates an great attention due to the surface area increase, and the consequent improved availability of active sites [5].

LDHs are extensively studied as sorbents due to their ion exchange capacity, reconstruction reactions and acid-base

E-mail address: rrojas@fcq.unc.edu.ar

http://dx.doi.org/10.1016/j.cej.2016.06.007
1385-8947/

buffering capacity (due to the dissolution reactions of LDH layers at low pH values) [6]. LDHs structure is derived from that of brucite ($Mg(OH)_2$) and it is described as layers of edge-sharing octahedra, where divalent metal ions are partially substituted by trivalent ones. Consequently, the layers present a positive charge excess that is compensated by the introduction of anions between them [7]. The general formula of these compounds can be written as $[M^{II}_{1-x}M^{III}_x(OH)_2]^{x+}(A^{n-})_{x/n}{\cdot}y\ H_2O$, where M^{II} and M^{III} are the metal ions that constitute the layers and A^{n-} is the interlayer anion.

Although LDHs are mainly studied as scavengers of anionic pollutants, either organic [8] or inorganic [9], numerous studies on the heavy metal remediation capacity of LDHs have also been performed [10–14]. Heavy metal ions are eliminated by two main mechanisms: precipitation and chelation. In the first case, the dissolution reactions of LDH layers buffer the pH of the contaminated media, which induce the precipitation of the corresponding heavy metal hydroxides, either as part of an LDH phase or not [12]. In the case of chelation, the LDH sorbent is intercalated with a functional ligand that interacts with the heavy metal ion, which is incorporated to the interlayer of LDHs [11,15,16]. In addition to these main mechanisms, adsorption/surface complexation processes have also been proposed for heavy metal adsorption by these solids [17].

In the case of the precipitation mechanism, the uptake capacity and kinetics are mainly controlled by the dissolution behavior of LDHs [12,13], which, as a surface controlled reaction, is expected to be determined by their particle size [6]. LDHs are obtained in a wide size range, from a few tens nanometers [18] to several micrometers [19]. Nevertheless, the effect of particle size on the solubility of LDHs remains unexplored, as well as the consequences on the heavy metal scavenging capacity of these solids.

In this work, these aspects were studied in three solids with similar structure (studied by X-ray diffraction, infrared spectra and thermal analysis) and composition, but different size and morphology (determined by dynamic light scattering and scanning electronic microscopy). Their dissolution and Cu^{2+} uptake behavior was studied by kinetics and isotherms. The obtained results were modeled to determine the mechanism involved in these processes and compare the uptake capacity and affinity of LDHs with different size.

2. Materials and methods

Reagent grade chemicals (Baker, Anedra) were used with no previous purification. All solutions were prepared with purified water (18 MΩ Milli Q, Millipore System). Unless otherwise stated, all experiments were performed at room temperature. Synthetic hydrotalcite (DHT-6) was gently provided by Kyowa Kagaku Kogyo Co., Ltd., Japan.

2.1. Synthesis of LDH nanoparticles

LDH nanoparticles intercalated with carbonate were obtained by a method involving separate nucleation and aging steps, similar to that described by Xu and coworkers [20]. Briefly, a solution containing the metal salts (50 mL) was poured into an alkaline solution containing Na_2CO_3 (0.2 L) under vigorous stirring induced by an Ultraturrax T18 BASIC agitator at 25,000 rpm. The Mg/Al ratio in the initial metal ions solution was 3:1 ($[Al^{3+}] = 0.2$ mol L^{-1}), while the $[OH^-]/[Mg^{2+} + Al^{3+}]$ was 2.2 and the $[CO_3^{2-}]/Al$ ratio was 1 in the alkaline solution. The obtained solid was immediately separated from the supernatants by centrifugation, washed 3 times with water and dispersed into 0.2 L of water by magnetic stirring for 24 h. The sample thus obtained was named LDH-NPs. Another sample was obtained as previously described but an additional step of aging by hydrothermal treatment (HT) at 80 °C for 4 h was added (LDH-NPs-HT). The synthesized samples and micro-sized LDH provided by Kyowa (DHT-6, from here on named LDH-μm) were stored as dispersions (10 g L^{-1}) in closed bottles.

2.2. Particle size and morphology

The hydrodynamic apparent diameter (d) and zeta potential (ζ) of the samples were determined by dynamic light scattering (DLS) and electrophoretic light scattering (ELS) measurements, respectively, using a Delsa Nano C instrument (Beckman Coulter). The measurements were performed in 1 g L^{-1} dispersions of the corresponding samples in 5 mmol L^{-1} NaCl solution, ultrasonically dispersed for 30 min. d values were obtained from the autocorrelation function ($g^{(2)}$) using the cumulants method and the size distributions were obtained by the CONTIN method, while electrophoretic mobilities were converted to ζ using the Smoluchowski equation. Scanning electron microscopy (SEM) images were obtained in a FE-SEM Σigma instrument on samples covered with a Cr layer. The samples were prepared placing 0.05 mL of 0.1 g L^{-1} dispersions of the samples on the holder, which was dried at 50 °C without further manipulation.

2.3. Structural characterization

50 mL of each dispersion were lyophilized in order to perform the structural characterization of the samples. Mg and Al contents were determined by atomic absorption spectrometry in a Varian AA240 instrument. The samples were dissolved in HNO_3 and afterwards diluted to meet the calibration range. Thermogravimetric and differential thermal analyses (TG/DTA) were carried out in a Shimadzu DTG 60 instrument in flowing air and at a heating rate of 10 °C/min. Powder X-ray diffraction (PXRD) patterns were recorded in a Phillips X'pert Pro instrument using a CuKα lamp ($\lambda = 1.5408$ Å) at 40 kV and 40 mA in step mode (0.05°, 1.2 s). FT-IR spectra were measured in a Bruker IFS28 instrument using KBr pellets (1:100 sample:KBr ratio).

2.4. LDHs dissolution

LDH dissolution at equilibrium was studied in 1 g L^{-1} LDH dispersions in 5 mmol L^{-1} NaCl (to fix the ionic strength) with increasing [HCl] (up to 35.2 mmol L^{-1}). The dispersions thus obtained were agitated for 48 h in an orbital shaker and pH was determined as previously described.

The kinetics of LDH dissolution was studied in 1 g L^{-1} LDH dispersions in 5 mmol L^{-1} NaCl at two [HCl] (0.88 and 8.80 mmol L^{-1}). Once the LDH particles were added, the dispersion was continuously agitated and the pH was measured every 90 s using a Titrando 905 automatic titrator (Metrohm) controlled by Tiamo software and coupled to a Metrohm 9.0262.100 combined pH electrode. The pH values were converted to proton uptake, $\Gamma_H = ([H^+]_0 - [H^+]_t) * V/m$, where $[H^+]_0$ and $[H^+]_t$ are proton concentration at t = 0 and at a given time t, V is the dispersion volume and m is the sample mass.

The Γ_H vs. t curves were fitted with the following equations [6,11,21,22]

$$\text{Zero order}: \Gamma_H = \Gamma_{H,0} + k_0 \cdot t \quad (1)$$

$$\text{Diffusion}: \Gamma_H = \Gamma_{H,0} + k_D \cdot t^{0.5} \quad (2)$$

$$\text{First order}: \ln \Gamma_H = n\Gamma_{H,0} + k_1 \cdot t \quad (3)$$

$$\text{Second order}: \frac{1}{\Gamma_H} = \frac{1}{\Gamma_{H,0}} + k_1 \cdot t \quad (4)$$

$$\text{Shirinking particle}: 1-(1-X)^{1/3} = k_{SP}\cdot t + C \quad (5)$$

where $X = \Gamma_H/\Gamma_{H,\,max}$ ($\Gamma_{H,\,max}$ is the proton uptake for a total LDH dissolution) and C is the intercept.

At t = 0, for this last model:

$$\Gamma_{H,0} = \Gamma_{H,max}\cdot(1-(1-C)^3) \quad (6)$$

2.5. Cu^{2+} uptake by LDHs

Cu^{2+} ion removal by the LDH samples was studied as a function of the metal ion concentration. The experiments were performed in 1 g L^{-1} dispersions of the corresponding samples in 5 mmol L^{-1} NaCl, 0.88 mmol L^{-1} HCl solutions with increasing initial concentration of Cu^{2+} ($[Cu]_0$, up to 10 mmol L^{-1}). These dispersions were allowed to equilibrate for 10 days under gentle up and down shaking. Then, the pH of the media and the equilibrium concentration ($[Cu]_{eq}$) in the supernatants were determined. $[Cu]_{eq}$ was determined by atomic absorption spectrometry (λ = 324.8 nm), as previously described.

The experimental data were fitted with the following equations [23]:

$$\text{Langmuir model}: \frac{[Cu]_{eq}}{\Gamma_{Cu}} = \frac{1}{K_L\Gamma_{Cu,max}} + \frac{[Cu]_{eq}}{\Gamma_{Cu,max}} \quad (7)$$

$$\text{Freundlich model}: \Gamma_{Cu} = K_F[Cu]_{eq}^{1/n},\ \ln\Gamma_{Cu} = \ln\ K_F + \frac{1}{n}\ln[Cu]_{eq} \quad (8)$$

where Γ_{Cu} is Cu^{2+} uptake, calculated as $\Gamma_{Cu} = ([Cu]_0 - [Cu]_{eq})\cdot V/m$, and $\Gamma_{Cu,max}$ is the maximum uptake capacity.

The kinetics of the uptake process was determined under the same conditions and selecting 1 mmol L^{-1} as the initial Cu^{2+} concentration. At defined times, the pH of the dispersions was measured and portions were withdrawn and filtered to determine $[Cu^{2+}]$ as previously described. Γ_{Cu} vs t curves were modeled with the same models than those presented in Section 2.4.

3. Results and discussion

3.1. Particle size and morphology

The proposed synthesis methods were successful on obtaining samples that presented different size distribution (Fig. 1) and morphology (SEM images in Fig. 2). The *d* values of LDH-NPs and LDH-NPs-HT were in the nano-scale (70 ± 7 and 135 ± 5 nm, respectively) while LDH-μm exhibited a *d* value around $4 \pm 1{\cdot}10^3$ nm. The polydispersity of LDH-NPs and LDH-NPs-HT samples were also lower than that of LDH-μm, which reflected in their size distribution, particularly narrow for LDH-NPs-HT. According to Xu and co-workers [24], the aging step is essential to produce monodisperse nanoparticles with low particle size, which has been related to the increased thermal energy during the aging in hydrothermal conditions and the consequent total disaggregation of the particles. Nevertheless, nano-sized particles were obtained for LDH-NPs only by agitation at room temperature, which has been rarely reported [25]. On the other hand, the larger size and narrow particle distribution of LDH-NPs-HT particles was explained by the aging in hydrothermal conditions [26], which lead

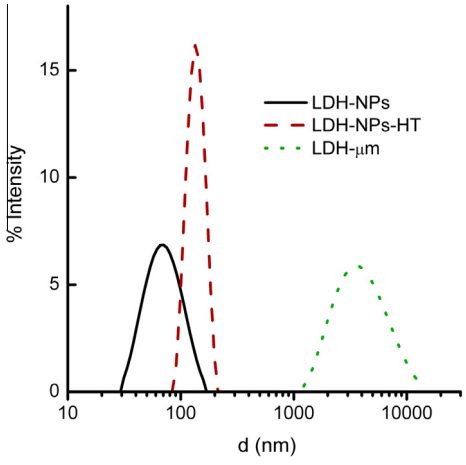

Fig. 1. Intensity size distribution of LDH samples.

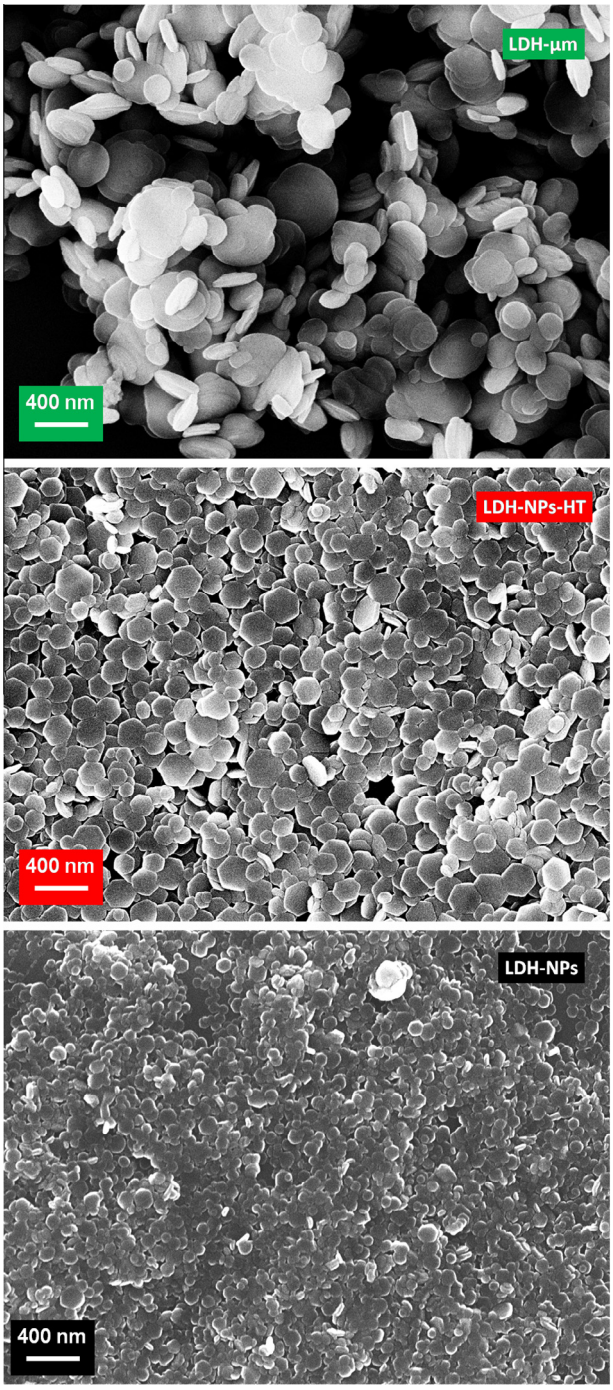

Fig. 2. SEM images of LDH samples.

to recrystallization and Ostwald ripening processes [27]. In good accord with that obtained by DLS, the SEM images (Fig. 2) showed increasingly large particles in the sequence LDH-NPs, LDH-NPs-HT and LDH-μm. Both LDH-NPs and LDH-NPs-HT particles exhibited planar nanoparticles, but the latter showed a more symmetric aspect and defined edges than the former. This indicated that LDH-NPs-HT was more crystalline than LDH-NPs due to the addition of the aging step in hydrothermal conditions. On the other hand, LDH-μm particles were larger and exhibited a round shape and a lower aspect ratio (diameter to thickness) than the other samples.

Positive ζ values were obtained for all samples: 38 ± 1, 49 ± 1 and 30 ± 1 for LDH-NPs, LDH-NPs-HT and LDH-μm, respectively. The positive charging of carbonate containing LDHs has been previously reported and explained by the interactions of carbonate at the particle surface of LDHs, which are mainly electrostatic [28,29]. The ζ values found in the literature for LDH nanoparticles [28] are larger than those in the micrometer range [30] (above and below 35 mV, respectively) and explain the larger disaggregation of the former. Also, they justify the colloidal stability of nano-sized LDHs, whose dispersions showed no sedimentation even 6 months after their synthesis. There was also a ζ increase by aging in hydrothermal conditions (from LDH-NPs to LDH-NPs-HT), which can be related to a more uniform distribution of Al^{3+} ions at the particle surface and edges [27,31].

3.2. Structural characterization

Portions of the sample dispersions were lyophilized to perform their structural characterization by PXRD and FT-IR spectroscopy (Supplementary material, Fig. S1A and B). The PXRD patterns of the samples showed peaks of carbonate intercalated Mg-Al LDH (powder diffraction file number 41-1428), which confirmed the presence of hydrotalcite-like compounds in all cases [19]. The peaks became wider in the order LDH-μm, LDH-NPs-HT and LDH-NPs, which indicated a decrease in the crystallite size [32], in good concordance with the decreasing particle size of the samples. This effect was particularly evident for peaks at $2\theta > 30°$, which almost disappeared for these samples. These peaks corresponded to planes with a basal component, which indicated the strong diminution of the layer size.

All FT-IR spectra exhibited a broad absorption band between 2200 and 4000 cm^{-1} (stretching vibration modes of the layer hydroxyl groups and interlayer water molecules), a band in the 1600–1700 cm^{-1} range (OH bending mode of water molecules) and several bands at wavenumbers lower than 1000 cm^{-1}, assigned to vibrational modes of the hydroxylated layers. The main carbonate band was centered at 1370–1380 cm^{-1}, while the CO_3^{2-}—H_2O bridging band was observed in the 2900–3100 cm^{-1} range [33,34].

DTA and TGA diagrams (supplementary material, Fig. S1C) exhibited the usual processes registered for the thermal decomposition of LDHs: removal of adsorbed (up to 100 °C) and interlayer (up to 225 °C) water, dehydroxylation and decarbonation (up to 500 °C). These last two processes presented overlapped endothermic peaks for LDH-NPs and LDH-NPs-HT, while two separated endothermic peaks were obtained for LDH-μm, which was associated with the larger size of the latter.

Based on the PXRD patterns and FT-IR spectra, the chemical composition of the samples (Table 1) was proposed considering that a single Mg-Al-LDH phase, completely intercalated with CO_3^{2-}, was obtained. The chemical formulae of the samples were quite similar, the Mg/Al ratio being near to the initial ratio of the synthesis solution in all cases. Then, the samples obtained were almost identical in composition and structure, the main difference being their morphology and, particularly, their particle size distribution.

Table 1
Elemental analysis and chemical formulae of LDH samples.

Sample	%Mg	%Al	Mg/Al	% H_2O[1]	Chemical formula
LDH-NPs	22.7	7.8	3.2	16.2	$Mg_{0.26}Al_{0.24}(OH)_2(CO_3)_{0.12}{\cdot}0.74{\cdot}H_2O$
LDH-NPs-HT	25.3	9.1	3.1	15.3	$Mg_{0.26}Al_{0.24}(OH)_2(CO_3)_{0.12}{\cdot}0.66{\cdot}H_2O$
LDH-μm	25.8	9.0	3.2	14.9	$Mg_{0.26}Al_{0.24}(OH)_2(CO_3)_{0.12}{\cdot}0.64{\cdot}H_2O$

[1] Obtained from the first weight loss of the thermogravimetric analysis curve.

3.3. LDHs dissolution

LDHs dissolution in acidic media [6,35] and Mg^{2+} leaching reactions in neutral and mildly alkaline media [35] are some of the main LDH proton uptake mechanisms that provide buffering capacity to these solids. Fig. 3 shows [HCl] vs. pH curves (A) and the proton uptake kinetics at two [HCl] (0.88, B, and 8.80 mmol L^{-1}, C). The pH of the LDH dispersions in water was around 9–10, which indicated some LDH dissolution in pure water. Although the main buffering capacity of LDHs was registered at pH below 5, there was also a small proton uptake up to pH = 5 that increased with decreasing particle size (Inset in Fig. 3A: from 1.8 to 3.5 mmol L^{-1} for LDH-μm and LDH-NPs, respectively). This proton uptake was assigned to Mg^{2+} leaching reaction, explained by the larger solubility of $Mg(OH)_2$ ($K_{PS} = 1.8{\cdot}10^{-11}$) compared to $Al(OH)_3$ ($K_{PS} = 1.3{\cdot}10^{-33}$). This reaction can be written as:

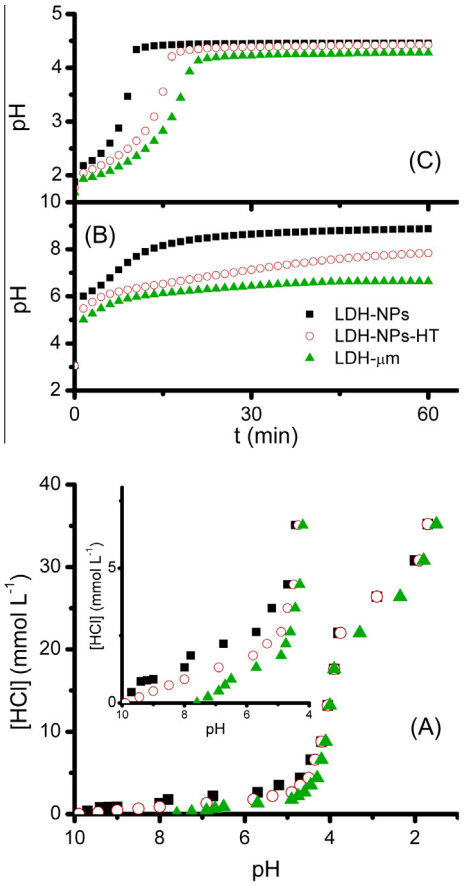

Fig. 3. HCl concentration ([HCl]) vs. pH curves of LDH dispersions in 5 mmol L^{-1} NaCl solution (inset: detail of the curves). Proton uptake kinetics at two [HCl]: 0.88 mmol L^{-1} (B) and 8.80 mmol L^{-1} (C).

$$Mg_{1-x}Al_x(OH)_2(CO_3)_{x/2}\cdot nH_2O_{(s)} + (2-3x)H^+_{(aq)} \rightarrow Mg^{2+}_{(aq)} + xAl(OH)_{3_{(am)}} + \frac{x}{2}\,CO_{3^{2-}(g)} + (n+2-3x)H_2O \quad (9)$$

The progression of this reaction was hindered by the formation of amorphous $Al(OH)_3$ as passive layer at the surface of LDH particles [35]. Consequently, a particle size reduction increased the access to Mg^{2+} ions, as this layer must cover a larger area.

As already mentioned, the larger proton uptake was produced in the 4–5 pH range, where initial [HCl] was around 20–25 mmol g^{-1}. This buffering capacity is due to the complete, congruent dissolution of LDHs according to the following reaction:

$$Mg_{1-x}Al_x(OH)_2(CO_3)_{x/2}\cdot nH_2O_{(s)} + (2+x)H^+_{(aq)} \rightarrow (1-x)Mg^{2+}_{(aq)} + xAl^{3+}_{(aq)} + \frac{x}{2}\,CO_{2(g)} + \left(n+\frac{x}{2}+2\right)H_2O \quad (10)$$

To study both Mg^{2+} leaching and LDH congruent dissolution, the proton uptake kinetics were studied at [HCl] = 0.88 and 8.80 mmol L^{-1} (Fig. 3B and C, respectively). For [HCl] = 0.88 mmol L^{-1}, a large pH gap was produced at the beginning of the experiment from around 2.8 to between 5 and 6 (depending on the particle size) due to the neutralization of the LDH dispersion. Then, a continuous pH increase with decreasing slope was obtained until a plateau was reached due to the formation of the $Al(OH)_3$ passive layer. In good concordance with the [HCl] vs pH curves, the equilibrium pH was above 5 in all cases and increased with the particle size of the samples (LDH-μm < LDH-NPs-HT < LDH-NPs).

A complementary behavior was obtained for [HCl] = 8.80 mmol L^{-1} experiments. Although a continuous pH increase was obtained in all samples, the maximum pH was almost the same and the pH gap between consecutive points increased until a point where the slope of the curve abruptly decreased and a plateau was reached. This indicated that, contrarily to that of kinetics at [HCl] = 0.88 mmol L^{-1} the equilibrium was almost exclusively determined by pH, as corresponded to the coherent dissolution of LDHs. The reaction rate increased with decreasing particle size (LDH-μm < LDH-NPs-HT < LDH-NPs) as demonstrated by the decreasing times to reach the equilibrium pH.

The pH values were converted, for this last set of experiments, to Γ_H values (scatters in supplementary material, Fig. S2). The proton uptake kinetics were modeled with zero, first and second order, diffusion and shrinking particle models. Similarly to that found in the literature [6,35,36], the best fits were obtained for the shrinking particle model (Table 2 and supplementary material, lines in Fig. S2) although good fits were also found for the zero order model. Both zero order and shrinking particle models indicate a surface controlled reaction, but the latter considers the surface area diminution due to the particle shrinking as the dissolution reaction proceeds. The good fittings by both zero order and shrinking particle models were explained by the incomplete LDH dissolution at this HCl concentration (around 30–40% of the initial mass), which led to a relatively reduced particle shrinking (see Table 2).

3.4. Cu^{2+} uptake by LDHs

For the study of Cu^{2+} uptake, an initial [HCl] = 0.88 mmol L^{-1} was selected, which provided an initial pH of 2.8. This pH is more likely in a natural media contaminated with heavy metal ions [2] and prevents the precipitation of the copper hydroxide [16]. At this [HCl], the samples presented increasing buffering capacity with decreasing particle size due to Mg^{2+} leaching, while LDH congruent dissolution was not produced (see Fig. 3B).

The Γ_{Cu} vs. $[Cu^{2+}]$ and pH vs. $[Cu^{2+}]$ curves showed (Fig. 4) showed a Γ_{Cu} increase and a pH decrease with increasing $[Cu]_{eq}$ in the whole measured range for all samples. The isotherms can be divided in two sections: at $[Cu]_{eq}$ below 0.4 mmol L^{-1} they showed a steep Γ_{Cu} increase to values that decreased with increasing particle size. Thus, the highest elimination percentages were reached in this stage (90%, 63% and 34% for LDH-NPs, LDH-NPs-HT and LDH-μm, respectively). Also, the dispersion pH diminished from 8.4, 6.5 and 5.7 for LDH-NPs, LDH-NPs-HT and LDH-μm, respectively, to a converging pH around 5.5. This high affinity sorption was assigned to $Cu(OH)_2$ precipitation in the neutral pH caused by LDHs buffering capacity due to Mg^{2+} leaching. This process was almost negligible for LDH-μm, which presented the largest particles, the highest stability and, consequently, led to pH values insufficient to produce $Cu(OH)_2$ precipitation. At $[Cu]_{eq}$ above 0.4 mmol L^{-1}, the Γ_{Cu} curve showed a decreasing slope with increasing $[Cu]_{eq}$ and increasing particle size, while similar pH values were obtained for all samples, decreasing below 5 at the largest $[Cu^{2+}]_{eq}$. The maximum Γ_{Cu} values obtained were 0.67, 0.51 and 0.10 mmol L^{-1} for LDH-Nps, LDH-NPs-HT and LDH-μm, in line with that found in the literature [10]. Thus, Gonzalez et al. [22] obtained Γ_{Cu} values around 2 mmol g^{-1} for chloride-intercalated LDHs without HCl addition, but the final pH of the uptake experiments were in the 8–9 range.

The slightly acid pH, inadequate to produce $Cu(OH)_2$ precipitation, and the lower affinity for Cu^{2+} ions indicated that a different uptake mechanism was produced at large $[Cu^{2+}]_{eq}$. In order to determine the mechanism operating in this stage, Cu^{2+} kinetics at $[Cu^{2+}]_0$ = 1 mmol L^{-1} were performed (Fig. 5). Cu^{2+} removal was slow and a plateau was reached after 48 h in all cases. Γ_{Cu} vs. t curves were fitted with the same models than for proton uptake kinetics (Table 3). The best fit was obtained for the diffusion model in all cases and the calculated Γ_{Cu} vs. t curves were included in Fig. 5. The kinetic constant increased with decreasing particle size due to the increase of the equilibrium Γ_{Cu} but the differences were greatly diminished when normalized by this factor. The proposed mechanism for Cu^{2+} uptake was the isomorphic substitution of Mg^{2+} by Cu^{2+} ions in the octahedral sites of LDH layers, also named diadochy [10,37]. This mechanism was enabled by the sim-

Table 2
Fitting parameters obtained for the proton uptake kinetics of LDH samples ([HCl] = 8.80 mmol L^{-1}, [NaCl] = 5 mmol L^{-1}, [LDH] = 1 g L^{-1}).

Model	Diffusion			Zero order			Shrinking particle			First order			Second order		
Sample	$\Gamma_{H,0}$[a]	k_D[b]	R^2	$\Gamma_{H,0}$[a]	k_Z[c]	R^2	$\Gamma_{H,0}$[a]	k_{SP}[d]	R^2	$\Gamma_{H,0}$[a]	k_1[e]	R^2	$\Gamma_{H,0}$[a]	$-k_2$[f]	R^2
LDH-CO_3-NPs	1.3	2.4	0.991	3.6	0.56	0.997	3.5	12.3	0.999	4.0	9.5	0.976	4.2	14.4	0.949
LDH-CO_3-NPs/HT	1.8	1.8	0.994	3.7	0.37	0.995	3.5	8.0	0.998	4.0	6.2	0.973	4.1	10.7	0.936
LDH-CO_3	1.3	1.7	0.980	3.3	0.33	0.996	3.2	7.0	0.997	3.7	5.7	0.982	3.9	10.0	0.950

[a] mmol g^{-1}.
[b] mmol g^{-1} $min^{-0.5}$.
[c] mmol g^{-1} min^{-1}.
[d] 10^3 min^{-1}.
[e] 10^2 min^{-1}.
[f] g $mmol^{-1}$ min^{-1}.

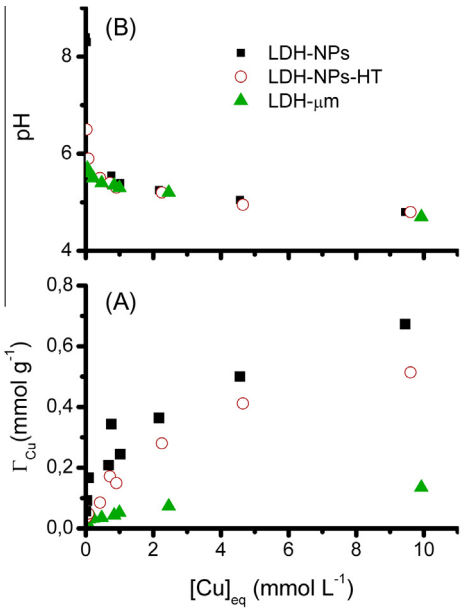

Fig. 4. Copper uptake (Γ_{Cu}, A) and pH (B) vs. $[Cu]_{eq}$ curves of LDH dispersions in 0.88 mmol L^{-1} HCl, 5 mmol L^{-1} NaCl solutions.

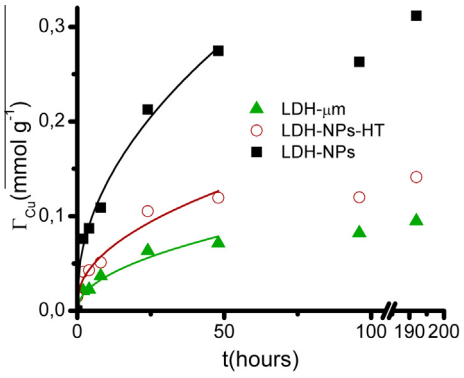

Fig. 5. Copper uptake kinetics for LDH dispersions in 1 mmol L^{-1} Cu^{2+}, 0.88 mmol L^{-1}HCl, 5 mmol L^{-1} NaCl solutions.

ilar ionic radius of both metal ions (86 and 87 pm for Mg^{2+} and Cu^{2+}, respectively) and the larger solubility of $Mg(OH)_2$ compared to $Cu(OH)_2$ (K_{SP} = 1.8·10^{-11} and 2.2·10^{-20}, respectively). According to the kinetic model, this isomorphic substitution was produced at the particle surface (more likely at the layers edges [35]) and, once all surface Mg^{2+} ions are substituted, migration of Mg^{2+} ions to the particle surface was necessary to maintain the reaction. This intraparticle diffusion [22] was the rate determining step of the uptake process and, consequently, the uptake rate increased with decreasing particle size due to the increased disponibility of sites, but the normalized rate was unaffected, as it is dependent on the diffusion distance, which is not affected by the particle size.

Table 4
Fitting parameters obtained for the Cu^{2+} sorption isotherms of LDH samples.

Model	Langmuir			Freundlich		
Sample	Γ_{max}[a]	K_L[b]	R^2	K_F[c]	1/n	R^2
LDH-CO_3-NPs	0.69	1.03	0.938	0.30	0.33	0.958
LDH-CO_3-NPs/HT	0.59	0.58	0.942	0.24	0.38	0.970
LDH-CO_3	0.15	0.80	0.945	0.05	0.34	0.945

[a] mmol g^{-1}.
[b] g mmol^{-1}.
[c] mmol g^{-1} (L mmol^{-1})$^{-1/n}$.

In order to complete the study of the Cu^{2+} uptake, the isotherms in Fig. 4 were fitted with the Langmuir and Freundlich models and the corresponding parameters are included in Table 4. These models are defined for surface adsorption and not for precipitation reactions. Nevertheless, they are useful to characterize the uptake process as well as the removal capacity of LDHs [13,21,23]. Freundlich model showed a slightly better fitting of the experimental curves in all cases, especially at high $[Cu]_{eq}$ (see the experimental and theoretical curves comparison included as supplementary material, Fig. S3). Langmuir model implies the presence of a finite number of active sites of equal adsorption energy, while the Freundlich implies an undefined number of active sites with different adsorption energies. For the diadochy mechanism, an undetermined number of LDH octahedrae were reactive and the adsorption energy was dependent on the distance from the particle surface. K_F indicated a higher uptake affinity with decreasing particle size but when normalized by the experimental maximum Γ_{Cu} value, the differences are small and also 1/n values were quite similar. This indicated that the affinity of LDHs for Cu^{2+} was quite similar and the main difference was the number of sites. If the thickness of the external stratum where incorporation was produced is considered similar for all the samples, the overall volume of this stratum, similarly to that of the exposed area, will increase with decreasing particle size, which explain the increasing number of sites.

4. Conclusions

Carbonate-intercalated Mg-Al nanoLDHs were obtained by a coprecipitation method with separate nucleation and aging stages. They exhibited similar composition and structure between them and with a micro-sized LDH, but they present different size and morphology. The particle size of these solids affected their buffering capacity in both neutral and acid media. In the first case, the buffering capacity, associated with Mg^{2+} leaching, increased with

Table 3
Fitting parameters obtained for Cu^{2+} uptake kinetics by LDHs ($[Cu]_0$ = 1 mmol L^{-1}, [HCl] = 8.80 mmol L^{-1}, [NaCl] = 5 mmol L^{-1}, [LDH] = 1 g L^{-1}).

Model	Diffusion					Zero order			Shrinking particle			First order			Second order		
Sample	$\Gamma_{Cu,0}$[a]	k_D[b]	R^2	$\Gamma_{Cu,48}$[a]	$k_D/\Gamma_{Cu,0}$	$\Gamma_{Cu,0}$[a]	K_0[c]	R^2	$\Gamma_{Cu,0}$[a]	k_{SP}[d]	R^2	$\Gamma_{Cu,0}$[a]	k_1[e]	R^2	$\Gamma_{Cu,0}$[a]	$-k_2$[f]	R^2
LDH-CO_3-NPs	1.4	3.82	0.987	27.5	13.8	7.5	0.45	0.959	7.4	1.7	0.965	8.2	2.79	0.905	8.5	2.0	0.831
LDH-CO_3-NPs/HT	1.0	1.69	0.956	11.9	14.2	3.3	0.21	0.872	3.3	0.7	0.877	4.2	2.47	0.869	4.3	3.6	0.836
LDH-CO_3	0.1	1.12	0.942	7.1	15.7	1.7	0.13	0.816	1.7	0.5	0.820	2.4	2.64	0.802	2.4	6.9	0.715

[a] 10^2 mmol g^{-1}.
[b] 10^2 mmol g^{-1} h$^{-0.5}$.
[c] mmol g^{-1} h^{-1}.
[d] 10^3 h^{-1}.
[e] 10^2 h^{-1}.
[f] 10^3 g mmol^{-1} h^{-1}.

decreasing particle size due to the increased surface area. In acid media, an increasing dissolution rate was obtained for decreasing particle size due to the surface control of LDHs dissolution rate. On the other hand, Cu^{2+} uptake mechanism depended on Cu^{2+} concentration: at low values, it was produced by $Cu(OH)_2$ precipitation and increased with decreasing particle size. At high ones, isomorphic substitution of Mg^{2+} ions in the octahedra of LDH layers (diadochy) was the main uptake mechanism, whose rate was controlled by the intraparticle diffusion of Mg^{2+} ions. The affinity of LDHs for Cu^{2+} ions was not dependent on particle size but there is a removal capacity increase with decreasing particle size due to the increased volume of the layer available for the Cu^{2+} ions incorporation.

Acknowledgements

Economic support by SeCyT-UNC, FonCyT (project number 12/0634), CONICET (PIP 11220120100575), and RED RIARTAS is gratefully acknowledged. The SEM images were obtained at the Laboratorio de Microscopía Electrónica y Análisis por Rayos X (LAMARX). The collaboration of Galatea Group for the copper determination by atomic absorption spectrometry is gratefully acknowledged.

Appendix A. Supplementary data

Supplementary data associated with this article can be found, in the online version, at http://dx.doi.org/10.1016/j.cej.2016.06.007.

References

[1] W.S. Wan Ngah, M.A.K.M. Hanafiah, Removal of heavy metal ions from wastewater by chemically modified plant wastes as adsorbents: a review, Bioresour. Technol. 99 (2008) 3935–3948, http://dx.doi.org/10.1016/j.biortech.2007.06.011.
[2] M.A. Hashim, S. Mukhopadhyay, J.N. Sahu, B. Sengupta, Remediation technologies for heavy metal contaminated groundwater, J. Environ. Manage. 92 (2011) 2355–2388, http://dx.doi.org/10.1016/j.jenvman.2011.06.009.
[3] J.-F. Peng, Y.-H. Song, P. Yuan, X.-Y. Cui, G.-L. Qiu, The remediation of heavy metals contaminated sediment, J. Hazard. Mater. 161 (2009) 633–640, http://dx.doi.org/10.1016/j.jhazmat.2008.04.061.
[4] R. Rojas, Applications of Layered Double Hydroxides on environmental remediation, in: A.C. Carrillo, D.A. Griego (Eds.), Hydroxides Synth. Types Appl., Nova Science Publishers, New York, 2012, pp. 39–71.
[5] M. Khajeh, S. Laurent, K. Dastafkan, Nanoadsorbents: classification, preparation, and applications (with emphasis on aqueous media), Chem. Rev. 113 (2013) 7728–7768.
[6] M.L. Parello, R. Rojas, C.E. Giacomelli, Dissolution kinetics and mechanism of Mg–Al layered double hydroxides: a simple approach to describe drug release in acid media, J. Colloid Interface Sci. 351 (2010) 134–139, http://dx.doi.org/10.1016/j.jcis.2010.07.053.
[7] V.A. Drits, A.S. Bookin, Crystal structure and X-ray identification of Layered Double hydroxides, in: V. Rives (Ed.), Layer. Double Hydroxides Present Futur, Nova Science, New York, 2001, pp. 39–92.
[8] J. Cornejo, R. Celis, I. Pavlovic, M.a. Ulibarri, Interactions of pesticides with clays and layered double hydroxides: a review, Clay Miner. 43 (2008) 155–175, http://dx.doi.org/10.1180/claymin.2008.043.2.01.
[9] K.-H. Goh, T.-T. Lim, Z. Dong, Application of layered double hydroxides for removal of oxyanions: a review, Water Res. 42 (2008) 1343–1368, http://dx.doi.org/10.1016/j.watres.2007.10.043.
[10] X. Liang, Y. Zang, Y. Xu, X. Tan, W. Hou, L. Wang, et al., Sorption of metal cations on layered double hydroxides, Colloids Surf. A Physicochem. Eng. Asp. 433 (2013) 122–131, http://dx.doi.org/10.1016/j.colsurfa.2013.05.006.
[11] R. Rojas, M.R. Perez, E.M. Erro, P.I. Ortiz, M.A. Ulibarri, C.E. Giacomelli, EDTA modified LDHs as Cu^{2+} scavengers: removal kinetics and sorbent stability, J. Colloid Interface Sci. 331 (2009) 425–431, http://dx.doi.org/10.1016/j.jcis.2008.11.045.
[12] R. Rojas, Copper, lead and cadmium removal by Ca Al layered double hydroxides, Appl. Clay Sci. 87 (2014) 254–259, http://dx.doi.org/10.1016/j.clay.2013.11.015.
[13] M.A. Gonzalez, I. Pavlovic, R. Rojas-Delgado, C. Barriga, Removal of Cu^{2+}, Pb^{2+} and Cd^{2+} by layered double hydroxide-humate hybrid. Sorbate and sorbent comparative studies, Chem. Eng. J. (2014), http://dx.doi.org/10.1016/j.cej.2014.05.132.
[14] M. Sun, Y. Xiao, L. Zhang, X. Gao, W. Yan, D. Wang, et al., High uptake of Cu^{2+}, Zn^{2+} or Ni^{2+} on calcined MgAl hydroxides from aqueous solutions: changing adsorbent structures, Chem. Eng. J. 272 (2015) 17–27, http://dx.doi.org/10.1016/j.cej.2015.03.009.
[15] T. Kameda, H. Takeuchi, T. Yoshioka, Uptake of heavy metal ions from aqueous solution using Mg–Al layered double hydroxides intercalated with citrate, malate, and tartrate, Sep. Purif. Technol. 62 (2008) 330–336, http://dx.doi.org/10.1016/j.seppur.2008.02.001.
[16] I. Pavlovic, M. Perez, C. Barriga, M.A. Ulibarri, Adsorption of Cu^{2+}, Cd^{2+} and Pb^{2+} ions by layered double hydroxides intercalated with the chelating agents diethylenetriaminepentaacetate and meso-2,3-dimercaptosuccinate, Appl. Clay Sci. 43 (2009) 125–129, http://dx.doi.org/10.1016/j.clay.2008.07.020.
[17] D. Zhao, G. Sheng, J. Hu, C. Chen, X. Wang, The adsorption of Pb(II) on Mg_2Al layered double hydroxide, Chem. Eng. J. 171 (2011) 167–174, http://dx.doi.org/10.1016/j.cej.2011.03.082.
[18] M. Chen, H.M. Cooper, J.Z. Zhou, P.F. Bartlett, Z.P. Xu, Reduction in the size of layered double hydroxide nanoparticles enhances the efficiency of siRNA delivery, J. Colloid Interface Sci. 390 (2013) 275–281, http://dx.doi.org/10.1016/j.jcis.2012.09.033.
[19] T. Hibino, H. Ohya, Synthesis of crystalline layered double hydroxides: precipitation by using urea hydrolysis and subsequent hydrothermal reactions in aqueous solutions, Appl. Clay Sci. 45 (2009) 123–132, http://dx.doi.org/10.1016/j.clay.2009.04.013.
[20] Z.P. Xu, G. Stevenson, C.-Q. Lu, G.Q.M. Lu, Dispersion and size control of layered double hydroxide nanoparticles in aqueous solutions, J. Phys. Chem. B 110 (2006) 16923–16929, http://dx.doi.org/10.1021/jp062281o.
[21] X. Liang, W. Hou, Y. Xu, G. Sun, L. Wang, Y. Sun, et al., Sorption of lead ion by layered double hydroxide intercalated with diethylenetriaminepentaacetic acid, Colloids Surf. A Physicochem. Eng. Asp. 366 (2010) 50–57, http://dx.doi.org/10.1016/j.colsurfa.2010.05.012.
[22] M.A. González, I. Pavlovic, C. Barriga, Cu(II), Pb(II) and Cd(II) sorption on different layered double hydroxides. A kinetic and thermodynamic study and competing factors, Chem. Eng. J. 269 (2015) 221–228, http://dx.doi.org/10.1016/j.cej.2015.01.094.
[23] R. Shan, L. Yan, K. Yang, Y. Hao, B. Du, Adsorption of Cd(II) by Mg–Al–CO_3- and magnetic Fe_3O_4/Mg–Al–CO_3-layered double hydroxides: kinetic, isothermal, thermodynamic and mechanistic studies, J. Hazard. Mater. 299 (2015) 42–49, http://dx.doi.org/10.1016/j.jhazmat.2015.06.003.
[24] Z.P. Xu, G.S. Stevenson, C.-Q. Lu, G.Q.M. Lu, P.F. Bartlett, P.P. Gray, Stable suspension of layered double hydroxide nanoparticles in aqueous solution, J. Am. Chem. Soc. 128 (2006) 36–37, http://dx.doi.org/10.1021/ja056652a.
[25] J.-M. Oh, S.-J. Choi, G.-E. Lee, J.-E. Kim, J.-H. Choy, Inorganic metal hydroxide nanoparticles for targeted cellular uptake through clathrin-mediated endocytosis, Chem. Asian J. 4 (2009) 67–73, http://dx.doi.org/10.1002/asia.200800290.
[26] X.-Q. Zhang, M.-G. Zeng, S.-P. Li, X.-D. Li, Methotrexate intercalated layered double hydroxides with different particle sizes: structural study and Controlled release properties, Colloids Surf. B. Biointerfaces 117C (2014) 98–106, http://dx.doi.org/10.1016/j.colsurfb.2014.02.018.
[27] X. Sun, S.K. Dey, Insights into the synthesis of layered double hydroxide (LDH) nanoparticles: Part 2. Formation mechanisms of LDH, J. Colloid Interface Sci. 458 (2015) 160–168, http://dx.doi.org/10.1016/j.jcis.2015.06.025.
[28] Z.P. Xu, Y. Jin, S. Liu, Z.P. Hao, G.Q.M. Lu, Surface charging of layered double hydroxides during dynamic interactions of anions at the interfaces, J. Colloid Interface Sci. 326 (2008) 522–529, http://dx.doi.org/10.1016/j.jcis.2008.06.062.
[29] R. Rojas, C. Barriga, C.P. De Pauli, M.J. Avena, Influence of carbonate intercalation in the surface-charging behavior of Zn–Cr layered double hydroxides, Mater. Chem. Phys. 119 (2010) 303–308, http://dx.doi.org/10.1016/j.matchemphys.2009.09.001.
[30] R. Rojas, F. Bruna, C.P. de Pauli, M.Á. Ulibarri, C.E. Giacomelli, The effect of interlayer anion on the reactivity of Mg–Al layered double hydroxides: improving and extending the customization capacity of anionic clays, J. Colloid Interface Sci. 359 (2011) 136–141, http://dx.doi.org/10.1016/j.jcis.2011.03.056.
[31] X. Sun, S.K. Dey, Insights into the synthesis of layered double hydroxide (LDH) nanoparticles: Part 1. Optimization and controlled synthesis of chloride intercalated LDH, J. Colloid Interface Sci. 458 (2015) 160–168, http://dx.doi.org/10.1016/j.jcis.2015.06.025.
[32] M. Herrero, F.M. Labajos, V. Rives, Applied Clay Science Size control and optimisation of intercalated layered double hydroxides, Appl. Clay Sci. 42 (2009) 510–518, http://dx.doi.org/10.1016/j.clay.2008.06.011.
[33] R. Rojas Delgado, C.P. De Pauli, C.B. Carrasco, M.J. Avena, Influence of MII/MIII ratio in surface-charging behavior of Zn–Al layered double hydroxides, Appl. Clay Sci. 40 (2008) 27–37, http://dx.doi.org/10.1016/j.clay.2007.06.010.
[34] J.T. Kloprogge, R.L. Frost, Infrared and Raman spectroscopic studies of layered double hydroxides (LDHs), in: V. Rives (Ed.), Layer. Double Hydroxides Present Futur., Nova Science Publishers, New York, 2001, pp. 139–192.
[35] M. Jobbágy, A.E. Regazzoni, Dissolution of nano-size Mg–Al–Cl hydrotalcite in aqueous media, Appl. Clay Sci. 51 (2011) 366–369, http://dx.doi.org/10.1016/j.clay.2010.11.027.
[36] S. Xu, M.C. Liao, H.Y. Zeng, X.J. Liu, J.Z. Du, P.X. Ding, et al., Surface modification and dissolution behavior of Mg–Al hydrotalcite particles, J. Taiwan Inst. Chem. Eng. 56 (2015) 174–180, http://dx.doi.org/10.1016/j.jtice.2015.04.013.
[37] S. Komarneni, N. Kozai, R. Roy, Novel function for anionic clays: selective transition metal cation uptake by diadochy, J. Mater. Chem. 8 (1998) 1329–1331, http://dx.doi.org/10.1039/a801631c.